World Conference on Timber Engineering Oslo 2023

FIRE CHARACTERISTICS OF A COMPARTMENT WITH EXPOSED CLT WALLS: AN EXPERIMENTAL INVESTIGATION USING THE STANDARD ISO 834 CURVE

Andrianos E. Koklas[1], Dionysios I. Kolaitis[2], Maria A. Founti[3]

ABSTRACT: Cross Laminated Timber (CLT) panels are increasingly used for building construction; in specific cases, the indoor surface of the CLT panels is required to be "exposed", thus making adequate fire protection of these elements a significant challenge. The main aim of this work is to experimentally determine the impact of an exposed CLT panel, in this case a ceiling, to the characteristics of a compartment fire. Experiments using either fire-resistant panels or a CLT exposed ceiling are performed in a test rig, corresponding to the 1/3 scale of the standard ISO 9705 compartment; a broad sensor network is installed to determine the main characteristics of the developing thermal- and flow-fields inside the compartment. In order to overcome certain limitations associated with achieving adequate levels of repeatability when a "realistic" time-dependent fire curve is used, a PID controller-based gas burner is employed; the ISO 834 standard temperature-time curve is used in all fire tests. The experimental results suggest that, as expected, when a CLT ceiling is used, the total fuel consumption at the burner is significantly lower. The thermal field inside the compartment exhibits certain differences, while the opening velocities were largely unaffected by the installation of the CLT ceiling.

KEYWORDS: Compartment fires, CLT, charring, fire engineering, measurements

1 INTRODUCTION

Wood construction is known to exhibit a range of advantages, compared to "conventional" construction methods (e.g. using concrete), in terms of seismic performance, cost and environmental footprint. However, due to the combustibility of wood, its fire behaviour is a major limiting factor in the development of new wooden buildings. Cross laminated timber (CLT) elements are load bearing elements, used either in vertical walls or slabs. In both of these cases, in order to enhance their fire performance, CLT elements can be encapsulated, i.e. covered by fire-resistant panels (e.g. gypsum plasterboards); however, due to aesthetic reasons, it is commonly required to leave "exposed" as much timber as possible. In the latter case, the adequate fire protection of the CLT elements poses significant challenges.

In order to investigate the fire behaviour of construction products, compartment fire tests are commonly used [1-5]. In these tests, the temporal evolution of the Heat Release Rate (HRR) usually follows either a "constant value" or a "time transient" profile. However, when a timber construction element is involved (e.g. an exposed CLT wall), the HRR inherently varies with time, due to the combustion process occurring in the wood, thus imposing an additional, time-varying fire load [1]. In the majority of fire tests using a "time transient" HRR profile, the fire source used is usually a wooden crib [2, 3, 4] or, in some rare cases, pertinent to large-scale compartments, actual furniture items [5]. However, both these options do not provide adequate levels of controllability and repeatability. In this context, this work presents a novel approach, where a series of fire tests are performed in a medium-scale compartment, equipped with a CLT wall, where the standard ISO 834 [6] time-temperature curve, commonly used in fire resistance furnace tests, is employed, aiming to ensure acceptable levels of repeatability.

This work is mainly aimed at investigating the effects of exposed CLT panels on the thermal characteristics of the fire developing inside a typical compartment. In this frame, two series of fire tests are performed in a medium scale compartment, one using an inert (non-combustible) material and the other using exposed CLT panels; the obtained measurements are then qualitatively and quantitatively compared.

2 EXPERIMENTAL SETUP

2.1 COMPARTMENT GEOMETRY

The fire compartment dimensions correspond to a 1/3 scale of the ISO 9705 [7] standard compartment, representing a typical room. The compartment's internal dimensions are 1200 mm (length) × 900 mm (width) × 900 mm (height); the door-type opening's dimensions are 266 mm (width) × 666 mm (height).

In the first test series, all sides of the compartment envelope (floor, walls, ceiling) were constructed using 20 mm thick fire-resistant ceramic boards; in the second

[1] Andrianos Koklas, National Technical University of Athens, Greece, andrianos.e.koklas@gmail.com
[2] Dionysios Kolaitis, National Technical University of Athens, Greece, dkol@central.ntua.gr
[3] Maria Founti, National Technical University of Athens, Greece, mfou@central.ntua.gr

https://doi.org/10.52202/069179-0233

series, the ceiling was replaced with a 3-layered (30 mm / 20 mm / 30 mm) 80 mm thick CLT panel (Figure 1), corresponding to a "fully exposed" CLT ceiling scenario.

***Figure 1**. Indicative photos of the test compartment with inert (left) and CLT (right) ceiling installed.*

2.2 FIRE SOURCE

In the majority of medium-scale and small-scale laboratory fire tests, the fire source used is either a gas burner, operating in "steady state" conditions, or a pool/crib fire burning freely. Both of these test methods exhibit certain drawbacks, i.e. the first is rather "unrealistic", while the latter is significantly lacking in repeatability. Aiming to investigate the possibility of using a gas burner (thus allowing adequate repeatability) in conjunction with a "realistic" time-temperature profile, a PID controller was developed in-house. In the fire tests presented here, the standard ISO 834 [1] curve was employed in order to comparatively assess the characteristics of the thermal- and flow-field developing inside the compartment, when an "inert" or a "combustible" (CLT) ceiling is used.

***Figure 2**. Indicative photo (top view) of the burner and the installed sensor network inside the compartment.*

A rectangular porous burner was used as the fire source. The burner dimensions were 125 mm (length) × 125 mm (width) × 60 mm (height) and it was positioned at the centre of the compartment's floor. The burner was fed with commercial propane (C_3H_8) (Figure 2). A digital mass-flow controller (Bronkhorst F-203AV-1M0-RGD-55-V) was used to measure and control the propane flow rate. More specifically, the average of the upper gas layer temperature and the ISO 834 standard temperature were estimated every second. The measured average upper gas layer temperature corresponded to the input of the PID controller, while the latter quantity was the set-point of the PID, changing every second; the PID controller's output was the signal to the mass flow controller. In this way, when the compartment temperature was higher than the corresponding ISO 834 value, the mass flow controller was instructed to reduce the fuel flow and vice versa.

2.3 SENSOR NETWORK

A broad network of measurement sensors was installed inside the test compartment to determine the main characteristics of the developing flow and thermal fields. Overall, 81 K-type thermocouples, 4 bi-directional velocity probes, 2 Pitot-static tubes, 4 heat flux meters, 1 continuous gas analyser and 3 digital flow meters were used.

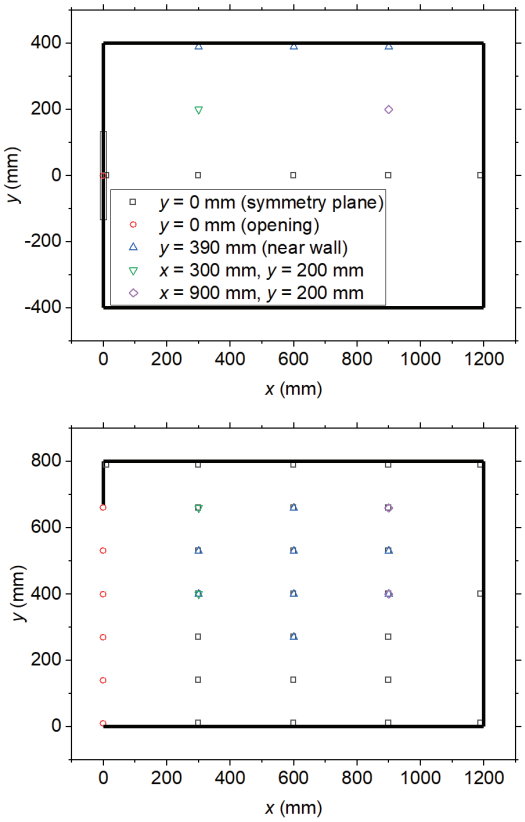

***Figure 3:** Spatial distribution of gas temperature and velocity measurement sensors, top view (top) and side view (bottom).*

The thermocouples were installed both inside the compartment (c.f. Figure 3), thus allowing measurement

https://doi.org/10.52202/069179-0233

of the gas phase temperature, as well as "inside" the ceiling (c.f. Figure 4) and compartment walls (c.f. Figure 5), at various locations across the thickness of the compartment envelope, aiming to record the temporal evolution of the thermal field developing "inside" the solid boundaries. When a CLT ceiling was tested, thermocouples were installed at the back (unexposed) side of each lamella (layer), corresponding to a distance of 30 mm, 50 mm and 80 mm from the exposed side, across the thickness of the CLT panel. The coordinate system used employs an axis origin that is located in the centre-line symmetry axis of the compartment (y = 0 mm), at the opening (x = 0 mm) on the floor level (z = 0 mm) (c.f. Figure 3).

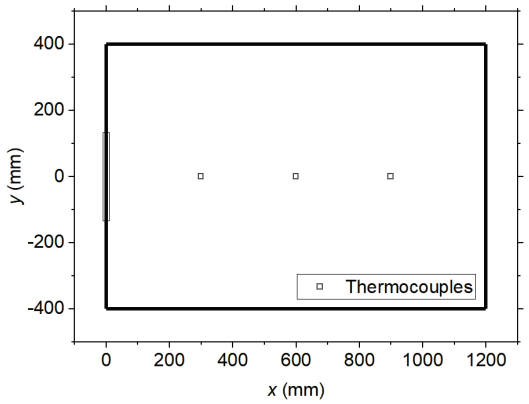

Figure 4: *Spatial distribution of the ceiling temperature measurement sensors.*

The gaseous combustion products were collected and a sample was fed to the gas analyser, where the oxygen, carbon dioxide and carbon monoxide concentrations were recorded. These measurements were later used to estimate the overall heat release rate, using the oxygen consumption calorimetry method (Equation 1) [8], where φ is the oxygen depletion factor, calculated using Equation 2. A brief description of all parameters that appear in Equations 1 and 2 is given in the Nomenclature.

$$\dot{Q} = \left[E_{O_2}\varphi - \left(E_{CO} - E_{O_2}\right)\frac{1-\varphi}{2}\frac{X_{CO}^{A^e}}{X_{O_2}^{A^e}} \right] \times \times \frac{\dot{m}_g}{1+\varphi(\alpha-1)}\frac{M_{o_2}}{M_a}\left(1-X_{H_2O}^{a}\right)X_{O_2}^{A^a} \quad (1)$$

$$\varphi = \frac{X_{O_2}^{A^a}\left(1-X_{CO_2}^{A^e}-X_{CO}^{A^e}\right)-X_{O_2}^{A^e}\left(1-X_{CO_2}^{A^a}\right)}{\left(1-X_{O_2}^{A^e}-X_{CO_2}^{A^e}-X_{CO}^{A^e}\right)X_{O_2}^{A^a}} \quad (2)$$

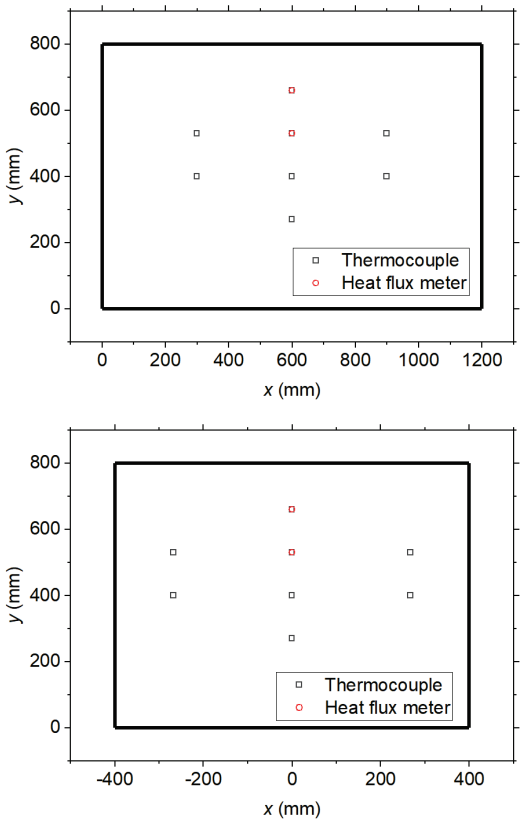

Figure 5: *Spatial distribution of the temperature and heat flux measurement sensors, at the side (top) and back (bottom) wall.*

2.4 MEASUREMENT UNCERTAINTIES

The gas temperatures were measured using K-type thermocouples connected to the signal acquisition system via extension wires. The systematic uncertainties of the thermocouples were a standard calibration uncertainty of ± 2.2°C or ± 0.75% of the measured value (the largest value is taken into account) for a 99% confidence interval (3σ), an uncertainty due to the wires and their extension of ± 2.2°C and a conversion uncertainty of ± 0.5%. The opening velocities were measured using bi-directional velocity probes and Pitot tubes. In terms of the systematic uncertainties, the bi-directional velocity probes exhibited a flow approaching uncertainty of ± 10% [4], a conversion uncertainty of ± 1% of the maximum pressure of the pressure sensor (10 Pa). The heat flux was measured using SBG01 water cooled heat flux meter. The calibration error is ± 3% of the measured value and the non-linearity error is ± 4% of the maximum heat flux (200 kW).

https://doi.org/10.52202/069179-0233

3 EXPERIMENTAL RESULTS

3.1 INERT ENVELOPE - REPEATABILITY

In the first series of fire tests, all sides of the compartment envelope were constructed using 20 mm thick ceramic boards. The standard ISO 834 time-temperature curve was used; the duration of each fire test was 3600 s. Measurements obtained at the upper gas layer of the compartment ($z \geq 660$ mm) were used to estimate the "average" temperature used in the PID controller to determine the required increase or decrease in the fuel flow.

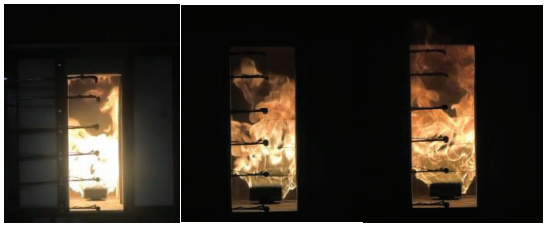

Figure 6: *Photos of a typical "inert" fire test, 600 s (left), 1800 s (middle) and 3600 s (right) after ignition.*

Initially, three identical fire tests have been performed, aiming to assess the "repeatability" of the test setup, based on the obtained measurements. In Figure 6, indicative images of the first "inert" (non-combustible envelope) fire test, using the standard ISO 834 time-temperature curve, are shown for three characteristic time instances, 600, 1800 and 3600 s after ignition. It is evident that the size of the developed flame covers a significant part of the compartment's height; in fact, the fuel mass flow rate at the 3600 s mark corresponds to a HRR value roughly equal to 100 kW.

Figure 7 depicts the temporal evolution of the standard ISO 834 fire curve against the experimentally measured values at the upper gas layer for the three "inert" experiments. It is evident that in all cases, the compartment temperature follows closely the standard ISO 834 curve.

Figure 8 depicts the temporal evolution of the gas temperature measurements obtained at three characteristic height levels, at a distance of x = 300 mm from the opening. The relatively small discrepancies observed among the three tests suggest that the developed test setup is capable of reaching increased levels of "repeatability".

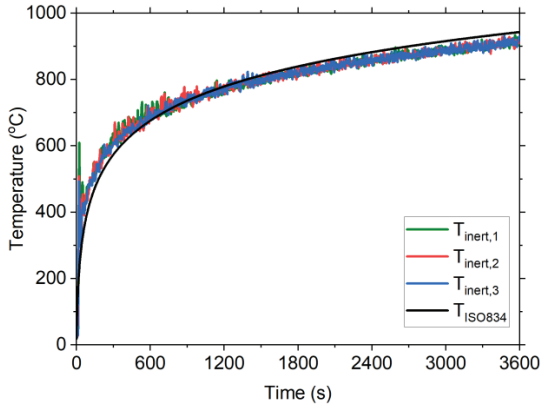

Figure 7*: Temporal evolution of average upper gas layer temperatures compared against the standard ISO 834 fire curve for the three "inert" experiments.*

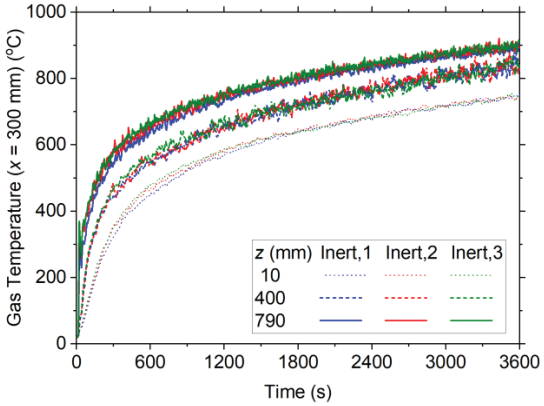

Figure 8*: Temporal evolution of indicative gas temperatures at a distance of x = 300 mm from the opening, for the three "inert" experiments.*

Figure 9 illustrates the spatial distribution of gas temperatures at the central symmetry plane ($y = 0$ mm) of the compartment, at three different time instants ($t = 600$ s, 1800 s and 3600 s). The grey box corresponds to the burner location, whereas the open rectangle (on the left, $x = 0$ mm) depicts the position of the compartment's door-type opening. As expected, the highest temperatures are observed near the centre of the compartment (above the burner) and at the upper gas layer (ceiling jet). Low temperatures close to the bottom part of the opening suggest the inflow of cold ambient air, providing oxygen for the fuel combustion process. Since standard ISO 834 curve imposes a monotonically increasing temperature profile, average compartment temperatures are gradually increasing with the elapse of time.

https://doi.org/10.52202/069179-0233

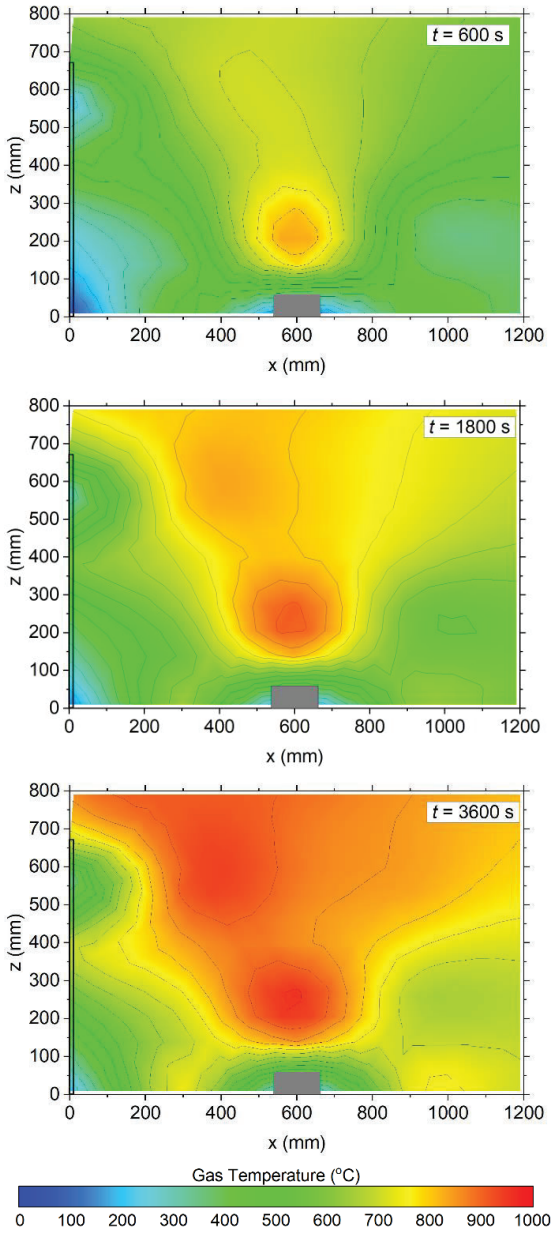

***Figure 9**: Spatial distribution of gas temperatures inside the compartment, 600 s (top), 1800s (middle) and 3600 s (bottom) after ignition.*

3.2 "EXPOSED" CLT CEILING

In the second series of fire tests, a Cross Laminated Timber (CLT) ceiling is installed in the test compartment, aiming to assess the impact on the fire characteristics. An 80 mm thick three-layer (1st layer 30 mm, 2nd layer 20 mm, 3rd layer 30 mm) CLT was used (Figure 10). Thermocouples were installed at the unexposed side of each layer, at two different axial locations (c.f. Figure 5). The fire test was terminated after 55 minutes, due to the collapse of the ceiling.

***Figure 10**: Inner view of CLT panel, installed at the compartment ceiling.*

Figure 11 shows characteristic views of the compartment where the CLT ceiling is installed, using the ISO 834 fire curve, at three distinct time instances. Although the temperature inside the compartment is similar in both test cases, in the CLT case the flame ejects from the opening faster than the non-combustible ceiling case. This is due to the additional pyrolysate gases released through the CLT ceiling. Since the upper gas layer is oxygen-lean, the pyrolysate gases cannot be burnt promptly; they have to exit the compartment, through the opening, in order for their combustion to be completed in the ambient air. By comparing Figures 6 and 11, it is evident that in the CLT case, flames appear also in the upper part of the compartment, due to the partial combustion of the pyrolysate gases released through the ceiling.

***Figure 11**: Photos of the "exposed CLT ceiling" fire test, 600 s (left), 1800 s (middle) and 3300 s (right) after ignition.*

In Figure 12, the temporal evolution of the average upper gas layer temperature in the two investigated test cases is compared against the standard ISO 834 curve. The "CLT" case exhibits some initial perturbations (due to inertia of the PID system that prevented the rapid adjustment of the fuel controller to the additional heat release due to CLT pyrolysis and combustion); however, after the 900 s mark, both cases follow closely the ISO 834 curve.

https://doi.org/10.52202/069179-0233

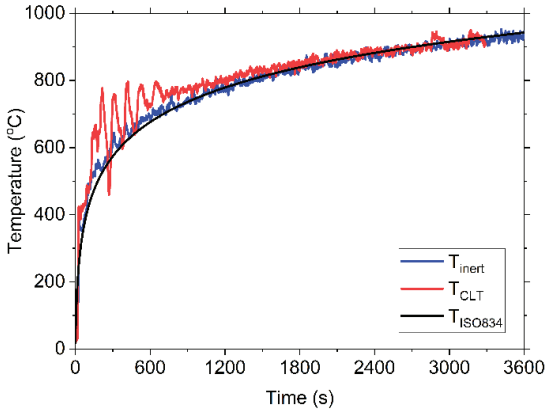

***Figure 12**: Temporal evolution of average upper layer gas temperatures compared against the standard ISO 834 fire curve.*

Figure 13 depicts the temporal evolution of the total fire HRR, corresponding to the sum of the HRR due to propane combustion and the HRR due to timber combustion, which was estimated using the oxygen combustion calorimetry method. After the initial period of fuel flow perturbations (t < 600 s), both cases result in similar HRR values. However, after the 2700 s mark, the total HRR in the CLT case is increased, thus suggesting that the increased HRR due to timber combustion cannot be counterbalanced anymore by the decreasing fuel flow to the burner; in fact, the gradually intensifying combustion of the CLT ceiling resulted in its partial collapse at 3300 s, thus prompting the early termination of the test.

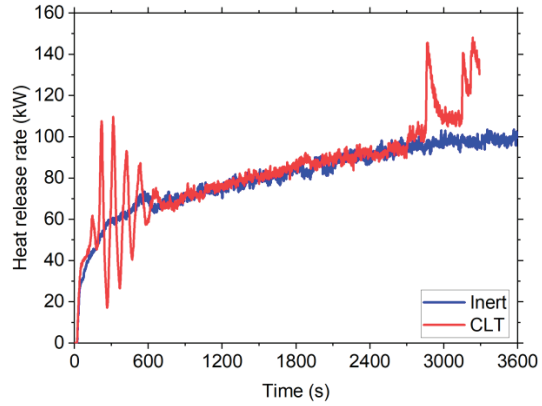

***Figure 13**: Temporal evolution of HRR for the "inert" and "CLT" test cases.*

Figure 14 illustrates the volumetric flow rate of the fuel, which was regulated by the PID controller; in Figure 15, the difference between the fuel flow rate in the "CLT" case, compared to the "inert" case is quantified. As expected, in order to achieve the ISO 834 curve, the "CLT" case requires a reduced fuel flow rate; in general, the reduction in the required fuel flow was more than 50% (Figure 15).

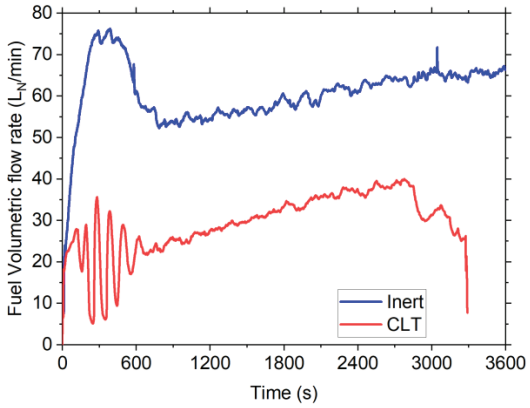

***Figure 14**: Temporal evolution of fuel volumetric flow rate for the "inert" and the "CLT" test cases.*

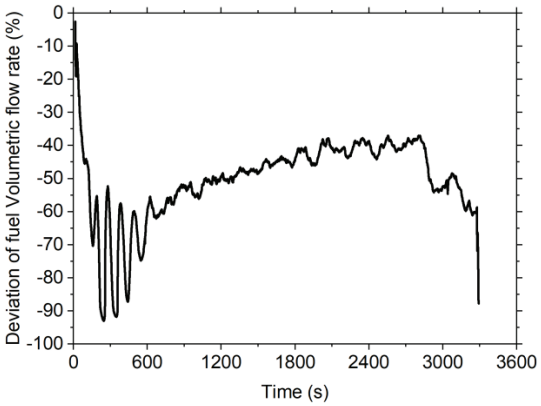

***Figure 15**: Temporal evolution of the deviation between the fuel flow rate between the "inert" and the "CLT" test cases.*

Figure 16 illustrates the spatial distribution of the gas temperature at the central plane of the compartment for three different time instances (t = 600s, 1800s and t = 3300s). Compared to the respective experimental results for the "inert" case (Figure 9), the "CLT" case results in a more "extended" region of higher temperatures close to the ceiling, due to the additional timber combustion processes that occur in this region.

https://doi.org/10.52202/069179-0233

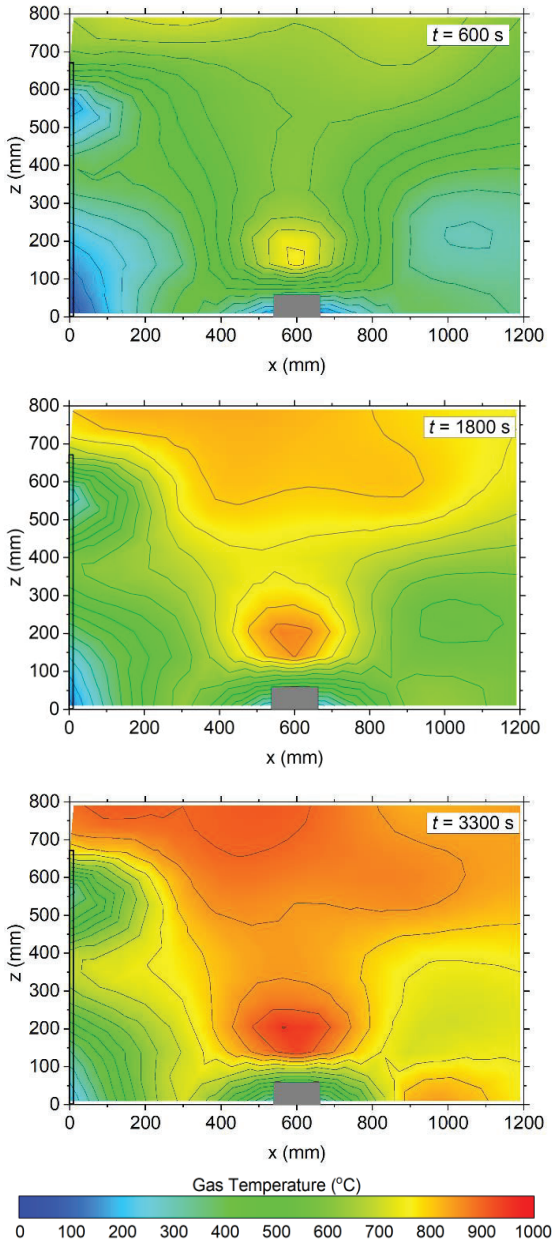

***Figure 16**: Spatial distribution of gas temperatures inside the compartment, 600 s (top), 1800s (middle) and 3600 s (bottom) after ignition.*

Figures 17-19 depict the temporal evolution of the gas temperature inside the compartment at three characteristic height levels (z = 140 mm, 400 mm and 660 mm above the floor); the measurements are provided for three locations across the compartment's symmetry axis, the first (x = 300 mm) close to the opening (Figure 17), the second at the centre (x = 600 mm) of the compartment (Figure 18) and the last close (x = 900 mm) to the back wall (Figure 19).

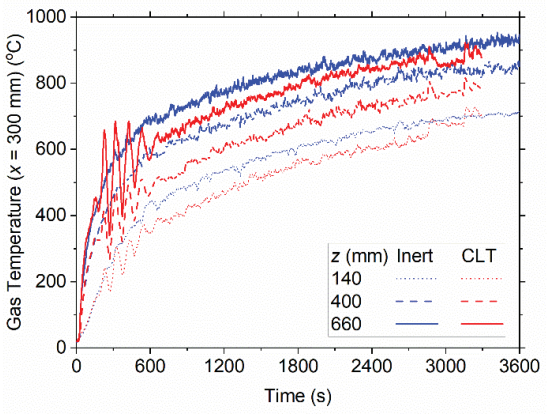

***Figure 17**: Temporal evolution of gas temperatures at three characteristic height levels, near the opening (x = 300 mm).*

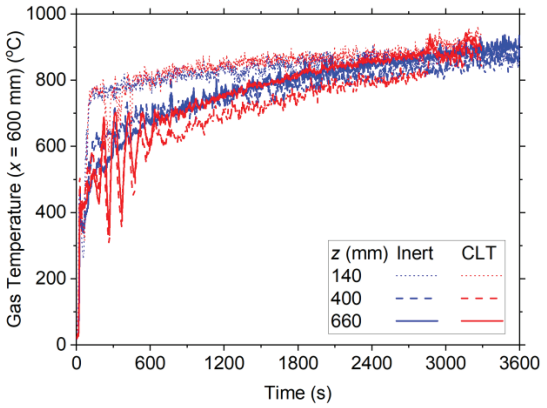

***Figure 18**: Temporal evolution of gas temperatures at three characteristic height levels, at the centre of the compartment (x = 600 mm).*

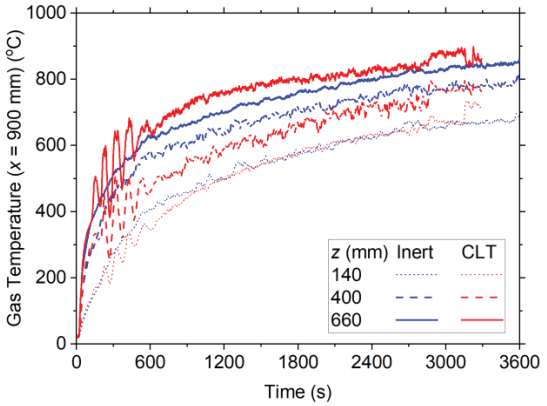

***Figure 19**: Temporal evolution of gas temperatures at three characteristic height levels, near the back wall (x = 900 mm).*

As expected, due to thermal buoyancy, gas temperatures are generally increasing with increasing height, with the

sole exception of gas measurements obtained just above the burner (z = 140 mm, Figure 20) which correspond to the peak temperature values inside the compartment (c.f. Figures 10 and 18). Since the pyrolysate gases close to the opening are ejected to the ambient air before being completely burnt, the average temperatures of the "inert" case are slightly higher than the corresponding values of the "CLT" case (Figure 19). However, at the "back" of the compartment (Figure 21), the thermal feedback from the burning CLT ceiling, in conjunction with the longer residence times of the produced pyrolysate gases allow a more "complete" combustion, thus leading to higher temperatures near the ceiling (z = 660 mm) for the "CLT" case.

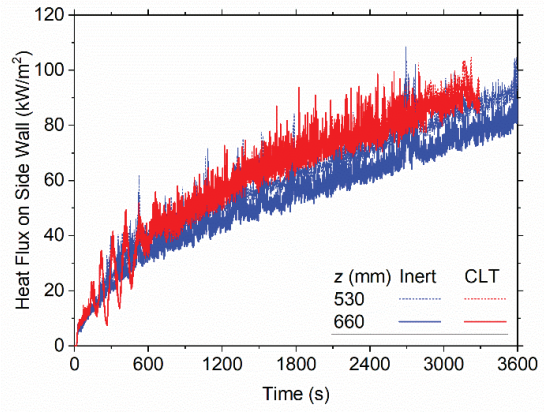

***Figure 20**: Temporal evolution of heat flux at the side wall (y = 400 mm).*

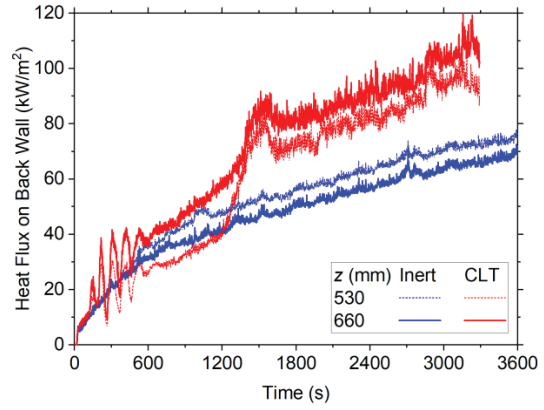

***Figure 21**: Temporal evolution of heat flux at the back wall (x = 1200 mm).*

Figures 20 and 21 show the temporal evolution of the incident heat flux at the side and the back wall, respectively. As expected, in all cases the measured heat flux values are increasing with time. For the "inert" test case, peak heat flux values are observed at a lower height level (z = 530 mm), due to the shorter flame developing in this case (c.f. Figures 6 and 11). However, in the "CLT" case, higher heat flux levels are recorded closer to the ceiling (z = 660 mm), where timber combustion takes place. In general, higher heat flux levels are observed in the "CLT" case compared to the "inert" case, due to the additional radiation from the flames appearing close to the ceiling (c.f. Figure 11).

Figure 22 depicts the effects of the combustible ceiling on the temporal evolution of the flow field developing at the opening plane. Positive velocity values suggest ambient air entering the compartment, whereas negative values signify combustion products exiting through the opening.

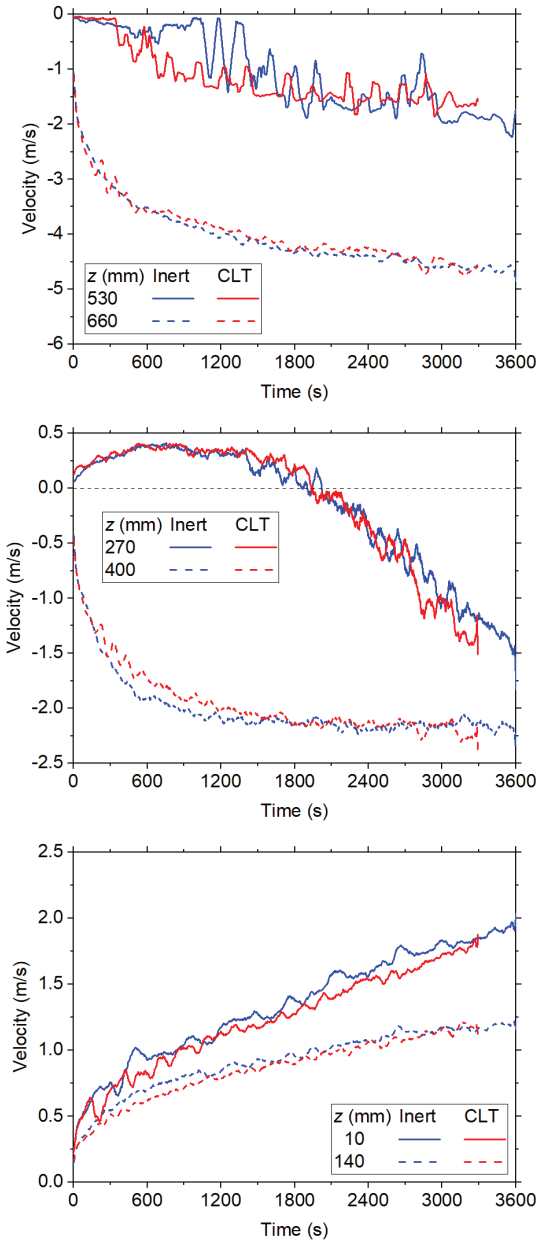

***Figure 22:** Temporal evolution of gas velocities in the upper (top), middle (middle) and lower (bottom) layer of the opening.*

https://doi.org/10.52202/069179-0233

As expected, at the top section of the opening (Figure 22, top), only negative velocity values are recorded, thus suggesting that the hot combustion products, concentrated under the ceiling, escape through the opening's lintel. The gradual increase of the compartment's temperature and, therefore, of the HRR, results in an increasing mass flow rate of the combustion products; as a result, the absolute values of the corresponding velocities are also increasing. Negative velocity values are recorded at the top half of the opening ($z > 300$ mm). During the first half of the fire test ($t < 1800$ s), velocity measurements obtained at a height of $z = 270$ mm (Figure 22, middle) suggest that ambient air is entering the compartment. However, as time goes by and the HRR is increased, the increasing mass flow rate of the hot combustion products results in a "reversal" of the flow direction at this specific height, thus leading to negative velocity values. At the lower part of the opening (Figure 22, bottom), the velocity of the incoming ambient air is monotonically increasing, due to the increasing HRR and, therefore, the need for oxygen.

In general, the CLT ceiling does not seem to significantly affect the measured velocity values. This is also evident in Figure 23, where the vertical velocity profiles at the opening, for three characteristic time instances, are shown. It is interesting to note as time goes by, due to the increasing HRR, the absolute values of both the incoming air and the outgoing combustion products are increased.

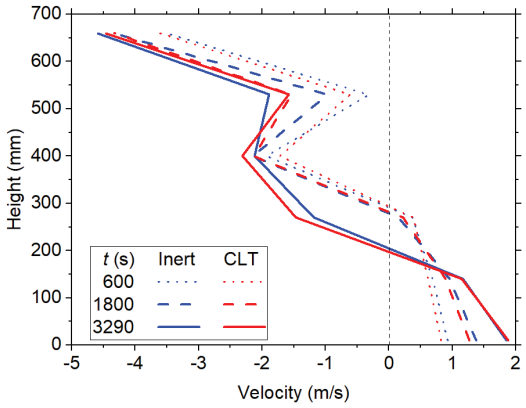

Figure 23: *Gas velocity profile in the opening at 600 s, 1800 s and 3600 s.*

Figure 24 depicts the recorded solid-phase temperatures across the thickness of the CLT ceiling. The distance from the opening ($x = 600$ mm vs. $x = 900$ mm) does not seem to significantly affect the CLT temperatures. According to the recorded temperatures at the unexposed side of the 1st layer, the charring front did not reach the second layer of the CLT ceiling. Near the 3000 s mark, the first CLT layer started to fall-off and the temperatures between the first and second lamella started to rise. The fall-off did not affect significant the temperatures measured between the 2nd and 3rd lamella.

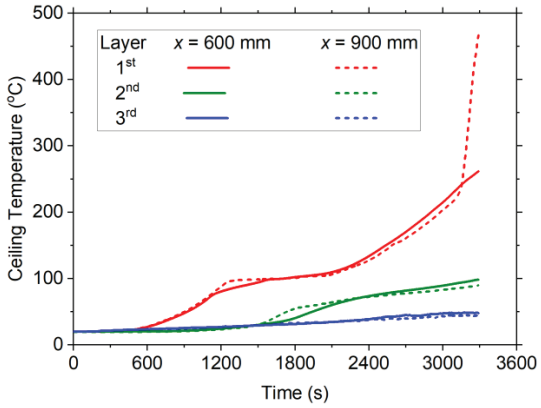

Figure 24*: Temporal evolution of solid-phase temperatures at the unexposed side of each lamella (layer) of the CLT panel.*

4 CONCLUDING REMARKS

In this work, two different series of laboratory experiments were conducted, aiming to assess the impact of installing an exposed CLT panel at the compartment's ceiling, on the characteristics of the thermal- and flow-fields developing inside the compartment, when the ISO 834 standard fire curve is used.

Based on the experimental observations made during the tests, the main effects of installing an exposed CLT ceiling are summarized below:

- The flames eject from the opening quite earlier, a fact that should be taken into account during the building design phase, e.g. suggesting potential additional requirements for the fire protection of façade systems.
- The fuel needed to reproduce the standard ISO 834 fire curve was about 50% less compared to the "inert" case. This fact highlights certain concerns, regarding the use of time-temperature curves for classification purposes, e.g. fire-resistance tests of combustible materials.
- Although the average compartment temperature was kept constant, in the case of the CLT ceiling, higher temperatures were observed at the back of the compartment (and, consequently, lower temperatures near the opening) compared to the respective measurements obtained for the non-combustible ceiling.
- The heat flux levels recorded inside the compartment were significantly higher in the case of the exposed CLT ceiling.
- The addition of the CLT ceiling does not seem to have any significant affect to the exhaust gas and the incoming air velocities.

The presented experimental campaign will be extended in the future, aiming to investigate the effects of alternative exposed CLT panel configurations, i.e. exposed ceiling, one exposed side wall, two exposed side walls, exposed ceiling and one side wall and exposed ceiling and two side

https://doi.org/10.52202/069179-0233

walls, as well as the effects of different fire curves (e.g. temperature-time, HRR-time).

ACKNOWLEDGEMENTS

This work has been financially supported by the E.C. in the frame of the H2020-project "Build-in-Wood: Sustainable Wood Value Chains for Construction of Low-Carbon Multi-Storey Buildings from Renewable Resources" (Grant agreement No. 862820).

REFERENCES

[1] Crielaard, R., Van de Kuilen, J., Terwel, K., Ravenshorst, G., Steenbakkers, P. (2019). Self-extinguishment of cross-laminated timber. *Fire Safety Journal, 105*, 244-260. doi:10.1016/j.firesaf.2019.01.008

[2] Bartlett, A.I., Hadden, R.M., Hidalgo, J.P., Santamaria, S., Wiesner, F., Bisby, L.A., Lane, B. (2017). Auto-extinction of engineered timber: Application to compartment fires with exposed timber surfaces. *Fire Safety Journal, 91*, 407-413. doi:10.1016/j.firesaf.2017.03.050

[3] Hadden, R.M., Bartlett, A.I., Hidalgo, J.P., Santamaria, S., Wiesner, F., Bisby, L.A., Lane, B. (2017). Effects of exposed cross laminated timber on compartment fire dynamics. *Fire Safety Journal, 91*, 480-489. doi:10.1016/j.firesaf.2017.03.074

[4] Wiesner, F., Bisby, L.A., Bartlett, A.I., Hidalgo, J. P., Santamaria, S., Deeny, S., Hadden, R.M. (2019). Structural capacity in fire of laminated timber elements in compartments with exposed timber surfaces. *Engineering Structures, 179*, 284-295. doi:10.1016/j.engstruct.2018.10.084

[5] Li, X., Zhang, X., Hadjisophocleous, G., McGregor, C. (2014). Experimental study of combustible and non-combustible construction in a natural fire. *Fire Technology, 51*(6), 1447-1474. doi:10.1007/s10694-014-0407-4

[6] ISO 834-1, Fire Resistance Test-Elements of Building Construction, Part 1: General Requirements, ISO, Geneva (1999).

[7] ISO 9705-1, Reaction to fire tests - Room corner test for wall and ceiling lining products - Part 1: Test method for a small room configuration, ISO, Geneva (2016).

[8] Janssens, M.L. (1991). Measuring rate of heat release by oxygen consumption. *Fire Technology, 27*(3), 234-249. doi:10.1007/bf01038449

NOMENCLATURE

Symbol	Unit	Description
α	-	Combustion expansion factor
E_{CO}	kJ/kg	Net heat release per unit mass of O_2 consumed for CO
E_{O_2}	kJ/kg	Net heat release per unit mass of O_2 consumed
M_a	kg/kmo1	Molecular weight of air
$\dot{m}_g$	kg/s	Mass flow rate of exhaust gas stream
M_{o_2}	kg/kmo1	Molecular weight of O_2
$\dot{Q}$	kW	Heat release rate
$X_{CO}^{A^e}$	-	CO mole fraction of the exhaust gas stream
$X_{CO_2}^{A^a}$	-	CO_2 mole fraction of ambient air
$X_{CO_2}^{A^e}$	-	CO_2 mole fraction of the exhaust gas stream
$X_{H_2O}^{a}$	-	H_2O mole fraction of ambient air
$X_{O_2}^{A^a}$	-	O_2 mole fraction of ambient air
$X_{O_2}^{A^e}$	-	O_2 mole fraction at the exhaust gas stream
φ	-	Oxygen depletion factor

https://doi.org/10.52202/069179-0233